1   **High-pressure autohydrolysis process of wheat straw for cellulose recovery**

2   **and subsequent use in PBAT composites preparation**

3   C. Fiorentini[a], A. Bassani[a,*], G. Duserm Garrido[a], D. Merino[b], G. Perotto[b], A.

4   Athanassiou[b], J. Peräntie[c], N. Halonen[c], G. Spigno[a]

5   [a]Department for Sustainable Food Process (DiSTAS), Università Cattolica del Sacro Cuore, Via Emilia Parmense,

6   84, Piacenza, 29122, Italy

7   [b]Smart Materials, Istituto Italiano di Tecnologia, Via Morego, 30, Genova, 16163 Italy

8   [c]Microelectronics Research Unit, Faculty of Information Technology and Electrical Engineering, University of Oulu,

9   P.O. Box 4500, FI-90014, University of Oulu, Finland

10   *Corresponding author: andrea.bassani@unicatt.it

11

12   Abstract

13   The effect of autohydrolysis (AH) temperature (165 °C, 195 °C, 225 °C) on the structure,

14   purity, and recovery yield of the cellulose residue isolated after additional alkaline and

15   bleaching steps from wheat straw, was investigated. The processes were quantified for

16   mass yields in the different steps and for antioxidants and sugars release during AH.

17   AH at 195 °C allowed for the highest cellulose residue yield (83.5%) with purity (~70%)

18   and structure similar to the other residues. FTIR and X-ray analyses showed straw

19   cellulose (SC) with a type II polymorphism and crystallinity index increasing with AH

20   temperature. SC obtained at the end of the entire fractionation process (SC-195°C)

21   starting from AH residue-195°C was tested as a reinforcing agent in different percentage

22   (0, 2 and 5 % by weight) in poly(butylene adipate-co-terephthalate) (PBAT) films. The

23   Young's modulus of the films increased by ~17% with 5 wt.% cellulose, while tensile

24   strength and elongation break decreased.

25

26   Keywords

1. Introduction

Being produced in high amount around the world every year, wheat straw is one of the most abundant crop residues and, due to its fibrous composition, it provides a plentiful renewable cellulose resource that can be used for the preparation of nanocomposites (Kalia et al., 2011).

Usually, a pre-treatment step of lignocellulosic biomass (such as wheat straw) is required to achieve separation of cellulose from the tight bond with hemicellulose and lignin. There are different types of pre-treatments to remove hemicellulose, and among these, diluted acid hydrolysis is the most effective one (Lee et al., 2014). However, among existing hydrolysis techniques, the autohydrolysis represents a potential interesting method for the pre-treatment of lignocellulosic materials, from both an economic and environmental point of view, as no chemicals other than water are required (Carvalheiro et al., 2009). This technique involves heating lignocellulosic materials at high temperature (up to over 200 °C) with compressed water, causing hydrolysis reactions like using a dilute-acid hydrolysis approach. Indeed, high temperature promotes the autoionization of water and the release of acetic acid from acetyl substituents of hemicelluloses with the subsequent formation of hydronium ions which initialize and catalyse the hydrolysis reactions (Garrote et al., 2003; Ruiz et al., 2011). Therefore, the liquid phase, obtained after autohydrolysis, is mainly composed of hemicelluloses-derived oligomers and sugars and related degradation products (e.g., furfural and hydroxymethylfurfural) and of acetic acid, as mentioned above (Delbecq et al., 2018). Moreover, liquid phase can also include other compounds, which come from acid-soluble lignin extractives and phenolic compounds, that can be recovered and used as antioxidants in food or as precursors for the production of flavorings (e.g., vanillin) (Bauer et al., 2012; De Abreu et al., 2012; Vadivel et al., 2017). However, the phenolic compounds extraction during autohydrolysis is highly affected by temperature

2

54 (Ballesteros et al., 2017). For this reason, some other extraction techniques are under

55 investigation. For instance, Arauzo et al. (Arauzo et al., 2020) tested three temperatures

56 (200 °C, 230 °C and 260 °C) for hydrothermal delignification to improve the recovery of

57 phenolic compounds from spent coffee grounds with ultrasound assisted extraction.

58 The next steps of alkaline hydrolysis and bleaching (with oxidizing agents) are needed to

59 separate cellulose and lignin, which are the main constituents of the remaining solid

60 phase. Indeed, alkaline hydrolysis disrupts the lignin structure, facilitating the cellulose

61 recovery and removes the residual hemicelluloses thanks to the saponification of the

62 cross-linkage present between lignin and hemicellulose (Sun and Cheng, 2002).

63 Furthermore, the subsequent use of an oxidation agent, such as organic peroxide, is

64 another method used to catalyse the delignification process by breaking the ring structure

65 of the lignin, improving the effects of alkaline pre-treatments (Lee et al., 2014). Lignin

66 and part of hemicellulose can be degraded by the oxidation agent depending on the

67 conditions of use. On the other hand, cellulose is slightly affected by treatments, and thus

68 it can be recovered to be valorised (Miron and Ben-Ghedalia, 1982; Ramos et al., 2008).

69 Indeed, cellulose has many applications in different industrial sectors like food,

70 pharmaceutical or, as reported by Trache et al. (Trache et al., 2016), can be used as

71 reinforcing agent in polymer composites for the packaging area.

72 The main focus of this study was to compare autohydrolysis pre-treatment conducted at

73 three different temperatures to assess the effect on the cellulose structure, yield, and

74 polymorphism of the cellulose fibres obtained at the end of the process and to test the

75 addition of such fibres (named as straw cellulose, SC) as a reinforcing agent in

76 poly(butylene adipate-co-terephthalate) (PBAT) films. The latter is gaining interest in

77 recent years due to its properties, such as biocompatibility, biodegradability, and

78 flexibility. However, the high strength generally required in the packaging sector limits

79 the use of PBAT, thus, the addition of SC can be a potential solution to increase its

80 mechanical properties (Botta et al., 2021). Moreover, the higher the crystalline index of

81 the cellulose obtained, the more appropriate it is to be used as a reinforcing agent

82 (Rasheed et al., 2021; Reis et al., 2014).

83 Finally, the liquid recovered from the autohydrolysis process was investigated in terms

84 of total phenolic content and antioxidant activity to evaluate its potential exploitation as

85 a high added value residue.

86

87 2. Materials and methods

88 The wheat straw (WS) used for this study was supplied by a farmer from Piacenza

89 (Northern Italy). The WS was directly milled with a lab hammer mill equipped with a 2

90 mm sieve (Thomas Scientific, Model 4 Wiley® Mill, U.S.A.).

91 PBAT in pellet form (Ecoflex® F Blend C1200, a commercial product of BASF SE,

92 Germany) was used as the matrix. Both polyoxyethylenesorbitan monolaurate (Tween®

93 20) and microcrystalline cellulose (STD-MCC) used in the FTIR analysis and for PBAT

94 films production were purchased from Sigma-Aldrich. Microcrystalline cellulose

95 (VIVAPUR® 105, JRS Pharma) was used for XRD analysis.

96 The standards and reagents used were the following: gallic acid (Fluka, Buchs,

97 Switzerland), Folin-Ciocalteu reagent (Fluka, Darmstadt, Germany), iron(II) sulfate

98 heptahydrate ($FeSO_4 \cdot 7H_2O$) (Carlo Erba), iron (III) chloride ($FeCl_3$), sodium carbonate

99 (Na_2CO_3), 6-hydroxy-2,5,7,8-tetramethylchroman-2-carboxylic acid (Trolox), 2,4,6-

100 tripyridyl-s-triazine (TPTZ), ethanol (96% v/v), sulfuric acid 96% and hydrochloric acid

101 (HCl) (Sigma-Aldrich, St. Louis, MO, USA).

102

103 2.1 *Wheat straw composition*

104 The WS was chemically characterized in terms of moisture, ashes, proteins, and fat

105 content, following specific methods (AOAC, 2007). In addition, the fibrous components

106 (lignin, cellulose, and hemicellulose) were evaluated according to the structural

107 carbohydrate analysis (Sluiter et al., 2010).

108

109 *2.2 Lignocellulosic fractionation*

110 For the cellulose recovery, WS was subject to a lignocellulosic fractionation process

111 similar to the one used by Bassani et al. (Bassani et al., 2020) with some modifications

112 (Figure 1). The first step of autohydrolysis (testing three different temperatures) was

113 adopted to replace the classic acid hydrolysis step.

114 The autohydrolysis (AH) was carried out in a high-pressure laboratory reactor

115 (*Highpreactor* BR-1000, 990 mL, Berghof, Germany) by inserting the milled WS (30 g)

116 and distilled water (solid to liquid ratio 1:20 w/v). The reactor was started with an average

117 heating rate of 5 °C/min until the set temperature was reached (165 °C, 195 °C, and 225

118 °C corresponding to 6, 11, and 24 bar pressures, respectively). The set temperature was

119 maintained for 15 min, setting the stirrer rotation at 150 rpm to homogenize the sample.

120 At the end of the 15 min, the heating was stopped, and the system was let cooling down

121 to approximately 70 °C (no more reaction occurs below this temperature) in a laboratory

122 environment at room temperature. Subsequently, the reactor was opened to promote faster

123 cooling of the sample. Then, the latter was taken out from the reactor and filtered to

124 recover both the solid, that was dried for 24 h at 60 °C, and the liquor, that was stored at

125 4 °C to be characterized. The entire process took about 190, 230 and 260 minutes for AH

126 at 165 °C, 195 °C, and 225 °C, respectively considering the heating phase at 5 °C/min,

127 the 15 minutes at the AH temperature and the final cooling phase to 70 °C.

128 The dried solid residue was weighed to calculate the step mass yield, then treated with an

129 alkaline solution of 4N NaOH (w/v) and successively, the recovered solid was washed

130 with distilled water until neutral pH, dried for 24 h at 60 °C and weighed to calculate the

131 step mass yield. To improve the effects of alkaline pre-treatments (Lee et al., 2014), a

132 bleaching step was carried out with 5% H_2O_2 (v/v) (adjusted to pH 11 with NaOH) under

133 static conditions at room temperatures for 24 h. The solid was then recovered through a

134 filtration step and washed with 50% acid acetic (v/v) followed by washing with distilled

135 water until neutral pH. The final cellulose residue was dried for 24 h at 60 °C and weighed

136 to calculate the total mass and cellulose residue yield. All the steps of the lignocellulosic

137 fractionation process were carried out in triplicate.

138

139 2.3 *Autohydrolysis liquor analysis*

140 *2.3.1 Total phenolic content*

141 The liquor recovered from the autohydrolysis process (AH liquor) was analysed for total

142 phenolic content (TPC) using the Folin-Ciocalteu assay (Bassani et al., 2020). The results

143 were expressed as mg GAE/g of dry matter (dm) of wheat straw (GAE, gallic acid

144 equivalent) using a calibration curve prepared with standard gallic acid in water (Fluka,

145 100-800 mg/L, $R^2 = 0.999$).

146

147 *2.3.2 Antioxidant activity (FRAP assay)*

148 The ferric reducing antioxidant power (FRAP) of the AH liquor was evaluated according

149 to the procedure described by Bassani et al. (Bassani et al., 2020). The results were

150 reported as µmol Fe(II)/g of dry matter (dm) of wheat straw using a calibration curve

151 obtained with $FeSO_4 \cdot 7H_2O$ in water (Carlo Erba, 0.2-2 mmol Fe(II)/L, $R^2 = 0.999$).

152

153 *2.3.3 Antioxidant activity (ABTS assay)*

154 The ability of the antioxidant compounds in the AH liquor to reduce the 2,2'-azino-bis(3-

155 ethylbenzothiazoline-6-sulfonic) acid (ABTS) radical was measured as reported by

156 Bassani et al. (Bassani et al., 2020). The results were calculated and expressed as µmol

157 Tr/g dry matter (dm) of wheat straw using a calibration curve obtained with a Trolox®

158 standard (Tr) in 50% ethanol (Sigma Aldrich, 100-500 mg Tr/L, $R^2 = 0.999$).

159

160   *2.3.4 Release of monosaccharides and acetic acid*

161 The concentration of free monosaccharides (glucose, xylose, and arabinose) was

162 evaluated on the AH liquors by enzymatic kits (Megazyme kit, K-FRUGL, K-XYLOSE

163 and K-ARGA). On the same samples, the content of free acetic acid was also measured

164 (Megazyme kit, K-ACETRM).

165

166 2.4 *Solid residue analysis*

167   *2.4.1 Structural carbohydrates*

168 The structural carbohydrates analysis was performed on both the samples obtained after

169 the autohydrolysis step (AH residues) and the solids resulting at the end of the entire

170 lignocellulosic fractionation process (straw cellulose) as described by Sluiter et al.

171 (Sluiter et al., 2010), with minor modifications.

172 The solid residue (0.6 g) was mixed with 3 mL of 72% (w/w) sulfuric acid, and the

173 mixture was incubated in an orbital shaker (Ski 4 Argolab) at 30 °C, for 60 min and 180

174 rpm. The obtained sample was diluted with 84 mL of distilled water to obtain a final

175 sulfuric acid concentration of 4% (w/w). The mixture was then autoclaved at 121 °C for

176 60 min. After cooling to room temperature, the liquid fraction was separated using

177 Whatman ashless filter paper (N° 589/3) and analysed for acid-soluble lignin (absorbance

178 reading at 320 nm, using the absorbance coefficient of 30 L/(g*cm)), while the acid-

179 insoluble lignin was calculated from the dried solid residue which was left after the

180 determination of moisture and ash content. The sum of these two fractions (%) was used

181 to calculate the total lignin percentage. The % of hemicellulose of the analysed solid

182 residue was estimated from the percentage of xylose in the liquors (Megazyme kit, K-

XYLOSE) multiplied by the correction factor of 0.88 for C-5 sugars (xylose and arabinose). In contrast, the percentage of cellulose was estimated from the percentage of glucose in the liquors (Megazyme kit, K-FRUGL) multiplied by 0.90 for C-6 sugars (glucose, galactose, and mannose).

Based on the composition of the WS and that of the solid residues (AH residue and straw cellulose), the cellulose, hemicellulose and lignin recoveries were calculated using the equations below as ratio of the cellulose/hemicellulose/lignin present in the solid after AH or at the end of the whole process, and the cellulose/hemicellulose/lignin present in the starting WS:

$$\% \ Cellulose \ recovery = \frac{g \ cellulose_{solid \ residue}}{g \ cellulose_{WSdm}} \times 100 = \frac{\% \ cellulose_{solid \ residue} \times \% \ process \ yield \times g_{WSdm}}{g_{WSdm} \times \% \ cellulose_{WSdm}} \tag{1}$$

$$\% \ Hemicellulose \ recovery = \frac{g \ hemicellulose_{solid \ residue}}{g \ hemicellulose_{WSdm}} \times 100 = \frac{\% \ hemicellulose_{solid \ residue} \times \% \ process \ yield \times g_{WSdm}}{g_{WSdm} \times \% \ hemicellulose_{WSdm}} \tag{2}$$

$$\% \ Lignin \ recovery = \frac{g \ lignin_{solid \ residue}}{g \ lignin_{WSdm}} \times 100 = \frac{\% \ lignin_{solid \ residue} \times \% \ process \ yield \times g_{WSdm}}{g_{WSdm} \times \% \ lignin_{WSdm}} \tag{3}$$

2.4.2 Scanning electron microscope (SEM) observation

The surface aspect of the three straw cellulose residues was evaluated using a scanning electron microscope system (Fei Quanta FEG 250 Esem) in high vacuum. The samples were processed with a mini deposition of Au (99.99% purity) by Sputtering Metal (Balzers MED 010) for high resolution metallization.

2.4.3 Fourier-transform infrared spectroscopy (FTIR)

FTIR spectroscopic analysis was carried out on both the AH residues compared to the original WS sample, and the straw cellulose (named as SC-165°C, SC-195°C and SC-

225°C) compared to a standard sample of microcrystalline cellulose (STD-MCC) (Sigma Aldrich).

The analysis was performed by Transmission on KBr pellets using a Vertex FTIR (Bruker). Pellets were prepared for each sample by incorporating approximately 1-2 mg of each sample over 150 mg of KBr salt.

Scans were performed with a resolution of 4 cm^{-1} in the 500-4000 cm^{-1} range. A background scanning for correction was performed before data collection.

2.4.4 X-ray analysis and crystallinity

The crystallinity of the three straw cellulose residues obtained at the end of the entire lignocellulosic fractionation process (SC-165°C, SC-195°C, and SC-225°C) was analysed by X-ray diffractometry (XRD).

The XRD measurements were obtained with Rigaku SmartLab (CoKα radiation), using commercial microcrystalline cellulose (STD-MCC) (VIVAPUR®, JRS Pharma) as a control. The samples were lightly compacted for XRD measurements and the corresponding crystallinity was evaluated by fitting (Bruker Topas software) cellulose polymorph II $(1\bar{1}0)$ (110), (020) and $(3\bar{1}\bar{1})/(3\bar{1}1)$ diffractions together with background and broad amorphous diffraction between $(1\bar{1}0)$ and (110) to the measurements results in 2θ range of 5-45°. The crystallinity (%) was determined from the ratio between fitted crystalline diffraction peak area and total diffraction (crystalline and amorphous) area as reported previously (Jin et al., 2016).

2.5 *Films production*

2.5.1 Preparation of the PBAT/cellulose films

PBAT/SC films were prepared by extrusion. Prior to use, the PBAT pellets, the SC-195°C and the STD-MCC were dried for 24 h at 40 °C. PBAT, cellulose (total mass 80 g,

234 cellulose content 0, 2, and 5 wt.%), and Tween 20 at 1 wt.% were mixed for a few minutes.

235 The mixtures were then placed again in the oven at 40 °C overnight.

236 Afterwards they were labeled according to the percentage of cellulose used (0, 2 and 5

237 wt.%) as PBAT, PBAT/SC-195°C-2, and PBAT/SC-195°C-5, respectively. In addition,

238 a PBAT composite containing 2 and 5 wt.% STD-MCC, labeled as PBAT/STD-MCC-2

239 and PBAT/STD-MCC-5, respectively, were prepared for comparison. Films from each

240 blend were prepared in a twin-screw extruder (Scamex) using a flat die with 10 cm width.

241 The temperature profile used in the extruder, between inlet and outlet, was from 150 °C

242 to 190 °C with a screw rotation speed of 70 rpm. After processing, the obtained films

243 were rolled and cooled to room temperature using a three rolls puller calander (Scamex).

244 Ultimately, before being characterized, the prepared films (about 2 m length, 5 cm width,

245 and 150 μm thick) were conditioned at 25 °C and 50% relative humidity for two days.

246

247 *2.5.3 Mechanical and morphological properties of the PBAT/cellulose films*

248 Mechanical properties of the composite films (PBAT/SC and PBAT/STD-MCC) were

249 measured by uniaxial tensile tests along the film extrusion direction on a dual column

250 testing machine (Instron 3365). Samples of 4 mm width and 25 mm useful length of the

251 conditioned films were stretched at a rate of 50 mm/min. Five measurements were

252 conducted for each film sample, and from the stress-strain curves, the values of Young's

253 modulus (MPa), tensile strength (MPa), and elongation at break (%) were calculated.

254 The surface of composite films was imaged by placing a small sample on a metallic stub

255 using conductive carbon tape. Cross section of the films was obtained by freeze fracturing

256 composite films in liquid nitrogen and attaching them with conductive carbon tape to a

257 90" mount stub. After that, all samples were coated with 10 nm of gold and analyzed on

258 a scanning electron microscope (JEOL JSM-6490LA) using a secondary electron detector

259   (SEI). The microscope was operated at 5 kV and 78 μA and the images were taken at a

260   magnification of 500×.

261

262   2.6 *Statistical analysis*

263   ANOVA analysis, with subsequent Tukey's significant difference test (p-value of 0.05),

264   was used to compare the data obtained from each experiment using Graphpad Prism

265   software (version 8.4.3). All the data obtained in triplicate were reported as mean ±

266   standard deviation (SD).

267

268   **3. Results and discussion**

269   3.1 *Wheat straw composition and process yield*

270   Table 1 shows the obtained chemical composition of WS. These results are in line with

271   those reported in the literature (Kootstra et al., 2009; Pérez et al., 2007; Saleem Khan and

272   Mubeen, 2012). As expected, the mainly fibrous component of this agricultural feedstock

273   is cellulose. Therefore, WS can represent a valid source for the recovery of cellulose.

274   The recovered mass yields (i.e., the ratio between the recovered grams and the initial

275   grams of sample) of the different hydrolysis steps adopted during the process are reported

276   in Table 2. The total recovery yields (%) were calculated as the product of the yields

277   obtained at the end of each treatment.

278   The total mass yields at the end of the process are around 37% for the tests at 165 °C and

279   195 °C, while for the test conducted at 225 °C, the yields are lower (around 22%) and as

280   expected, the autohydrolysis conducted at higher temperatures (225 °C) leads to a higher

281   degradation of the sample and lower mass yields (Table 2). These results are in agreement

282   with a study conducted by Pérez et al. (Pérez et al., 2007), where high pressure and high-

283   temperature water treatments were tested on wheat straw. In addition, it is interesting to

284   underline that the yield of alkaline step, in case of test at 195 °C, is higher than the others

285   leading to a possible future reduction in the usage of NaOH solution, with the related

286   environmental benefit. On the opposite, in case of test at 225 °C, the solid yield at alkaline

287   step is lower due to the harder operating conditions that have led to a structure loss of the

288   wheat straw, thus making it more easily hydrolysed. Finally, in case of test at 165 °C, the

289   residual hemicellulose and lignin in the solid after the autohydrolysis are degraded in the

290   alkaline hydrolysis step, leading to the lower solid yield.

291

292   3.2 *Autohydrolysis liquors analysis*

293   *3.2.1 Total phenolic content and antioxidant activity*

294   The interest in the recovery of phenolic compounds as added-value antioxidant

295   compounds has increased in recent times (Bauer et al., 2012; Garrote et al., 2004; Tilay

296   et al., 2008) and in the perspective of a process that generates few waste streams material,

297   TPC and the antioxidant capacity of the AH liquor were evaluated and reported in Table

298   3.

299   The yield of TPC (evaluated by Folin's assay) is higher in the sample obtained from the

300   autohydrolysis treatment at 225 °C. In general, a higher content of phenolic compounds

301   corresponds to a higher antioxidant power. This was confirmed by the FRAP and ABTS

302   assays, two assays that assess the ability of phenols to reduce iron and ABTS radicals,

303   respectively. Indeed, in line with the TPC, the treatment at 225 °C reveals the highest

304   reducing capacity for FRAP and ABTS assays. Therefore, the process of autohydrolysis

305   conducted at higher temperatures (225 °C) tends to better hydrolyse hemicellulose and a

306   fraction of the acid-soluble lignin (which is of phenolic nature), leading to a higher release

307   of phenolic compounds that are normally bound to the cell wall, without decreasing their

308   antioxidant power.

309

3.2.2 Release of monosaccharides and acetic acid

311 The content of monosaccharides released in the liquid after autohydrolysis is reported in

312 Table 4. An increase in xylose release can be noted after treatment at 195 °C compared

313 to 165 °C, indicating increased hydrolysis of hemicellulose. Further increasing the AH

314 temperature (225 °C) brought to a reduction in measured xylose levels probably due to

315 dehydration of D-xylose to furfural during the process (Oefner et al., 1992). In fact, due

316 to the presence of strongly acidic conditions, sugars can be dehydrated, pentoses are

317 transformed to furfural, and hexoses to hydroxyfurfural (Delbecq et al., 2018). In the

318 presence of these compounds, a possible polycondensation reaction may occur, resulting

319 in the formation of aromatic compounds, which are probably responsible for the observed

320 increase in TPC and antioxidant activity (Delbecq et al., 2018). These assumed reactions

321 can also be confirmed referring to the decomposition pathway of relevant organic

322 components of biomass reported by Wüst et al. (Wüst et al., 2020), in the range of 175

323 °C - 350 °C. Moreover, a condensation reaction with lignin is also likely to occur, leading

324 to the formation of pseudo-lignin, with several examples in literature (Cheng et al., 2018;

325 Hu et al., 2012; Hubbe et al., 2018).

326 In addition, we detected a reduction in the arabinose content with increasing AH

327 temperature. Carvalheiro et al. (Carvalheiro et al., 2009) observed a similar trend in the

328 liquid fraction obtained from the AH of WS conducted at different temperatures (150-

329 240 °C), further supporting the hypothesis of increased hydrolysis of hemicellulose as

330 temperature increases.

331 However, the amount of monosaccharides released (especially the glucose level) in the

332 liquor after AH did not change significantly between the different temperatures tested.

333 Indeed, fibres degrade more forming monosaccharides at higher temperatures, but the

334 latter can further degrade forming sugar degradation product (e.g., hydroxymethylfurfural

335 or methylfurfural) for both a longer treatment time (Bassani et al., 2020) and higher

336   temperatures treatments (Sidiras et al., 2011). For example, at 225 °C there is more

337   degradation of fibres, but at the same time also of monosaccharides to form sugar

338   degradation products. In addition, the measured concentrations of monosaccharides are

339   lower than those reported by Bassani et al. (Bassani et al., 2020) on a wheat straw sample

340   after treatment with 4.7% sulphuric acid in an autoclave at 121 °C for 45 min, confirming

341   that this process is less aggressive than acid hydrolysis in releasing monomers from fibres

342   (Ruiz et al., 2011).

343   Moreover, it can be noted that the pH tends to slightly decrease as the treatment

344   temperature increases. This behaviour is linked to the increase of the hydrolytic effect of

345   water, which increases with temperature. Indeed, pKa of water and its acid strength are

346   influenced by temperature. For instance, 5.0 and 6.14 are the pH or water at 200°C and

347   100°C, respectively. Water has a high dielectric constant, allowing it to ionize substances

348   and dissociate them. This effect leads to the break-up of the ester link between the acetyl

349   groups and xylose, causing their solubilization in the liquid fraction producing acetic acid

350   (Pérez et al., 2007). In fact, the level of released acetic acid following delignification of

351   the raw material increased slightly as the temperature increased. The sample treated at

352   the highest temperature (225 °C) produced the highest acetic acid value and, accordingly,

353   the lowest pH. This effect, which couples the acidification of the liquid and the

354   dissociation of water, enhanced the hydrolysis of hemicellulose (Carvalheiro et al., 2009;

355   Garrote et al., 2001).

356

357   3.3 *Solid residues characterization*

358   *3.3.1 Structural carbohydrates*

359   The recovery yields and the content of cellulose, hemicellulose, and lignin (acid-soluble

360   and insoluble lignin) of the samples obtained after the autohydrolysis and bleaching steps

361   are reported in Table 5.

362   The autohydrolysis at 225 °C, taking place at a higher temperature, is stronger and results

363   in more significant degradation of the sample, thus reducing the recovery yields,

364   including cellulose recovery yields. Moreover, the increase in temperature allowed us to

365   obtain a higher cellulose percentage content after the autohydrolysis step. In fact, the

366   samples obtained at 195 °C and 225 °C showed ~8% higher value (~46%) than the sample

367   obtained at 165 °C (~38%), since the high temperature led to a better solubilization of

368   hemicellulose (Fernández-Cegrí et al., 2012; Garrote et al., 2003).

369   Table 5 also suggests that the lignin content tends to increase with increasing AH

370   temperature. Several publications have shown that the relative percentage of acid-

371   insoluble lignin (Klason lignin) is greater in the acid pre-treated material than in the

372   starting untreated one. This is because only part of the material is natural lignin, while the

373   remaining material is lignin-like. This type of lignin-like structure, called pseudo-lignin,

374   could be synthesised through condensation reactions catalysed by acids on fragmented

375   polysaccharides or substitution reactions on the aromatic rings of lignin (Shinde et al.,

376   2018). This behaviour was already described in several studies conducted on agricultural

377   residues such as corn stover and WS subject to hydrothermal pre-treatments (Kaparaju

378   and Felby, 2010).

379   Thanks to the subsequent alkaline and bleaching steps, the hemicellulose and lignin

380   content could be further reduced in all three samples, leading to final residues (SC) with

381   higher purity in cellulose (around 70%), especially those from the AH conducted at a

382   higher temperature.

383

384   *3.3.2 Fourier-transform infrared spectroscopy (FTIR)*

385   FTIR is usually used to investigate the changes of chemical functional groups during pre-

386   treatments.

387   The FTIR spectra of WS and AH residues are shown in Figure 2a. The peak at 895 cm^{-1}

388   is assigned to b-(1-4)-glycosidic bond (C-O-C) (Abidi et al., 2014). The intensities of this

389   absorption peak, typical of cellulose, decreased for all the solid residues with increasing

390   temperature. This suggests that with increased temperature, the glycosidic bond is broken,

391   and cellulose is depolymerized. Moreover, the absorption band at 1060 cm^{-1} and 1515

392   cm^{-1} is unique to the samples obtained after the autohydrolysis process and can be

393   associated at out of plane vibration of aromatic C-H bonds, which may be caused by the

394   presence of the pseudo-lignin produced by dehydration, re-arrangement, and

395   condensation reactions of the sugars (Shinde et al., 2018).

396   Furthermore, the three cellulose bands between 1100 cm^{-1} and 1115 cm^{-1} are due to C-O-

397   C stretching of glucose and other sugars (often associated with pectin or hemicellulose)

398   that can be considered the degradation products of cellulose.

399   In addition, the absorption bands at 1245 cm^{-1} and 1734 cm^{-1}, associated with C=O

400   stretching of hemicellulose, are less intense at temperatures above 195 °C, as expected,

401   being hemicellulose degraded in processes at 195 °C and 225 °C. The autohydrolysis pre-

402   treatment at 165 °C did not degrade hemicellulose, and this is in line with the results

403   obtained with structural carbohydrate analysis (Table 5).

404   In the samples AH residues 165 °C, 195 °C, and 225 °C there is a shoulder that becomes

405   a peak at 1706 cm^{-1} that, together with the vibration at 1648 cm^{-1} more visible in these

406   three samples, is associated with the presence of conjugated carbonyl groups (Sun et al.,

407   2005; Zhang et al., 2010) produced by the hydrolysis of the hemicellulose and lignin.

408   The peak at 1610 cm^{-1} is a carbonyl stretching associated with absorbed water (Sun et al.,

409   2005).

410   As reported in Figure 2b, the FTIR spectra of the straw cellulose compared to STD-MCC,

411   do not show a substantial change among each other. The trend of the peak associated with

412   the glycosidic bond is similar between the three analysed samples. Therefore, the

413   subsequent basic hydrolysis and bleaching treatments seem to reduce the differences

414   found in the samples obtained after the AH step. The main feature of cellulose, between

415   950 cm^{-1} and 1150 cm^{-1}, became only slightly less defined. Moreover, the small

416   absorption band at 1640 cm^{-1} is attributed to the absorbed water in the cellulose (Liu et

417   al., 2005).

418

419   *3.3.3 Scanning electron microscope (SEM) observation*

420   SEM observations of the different straw cellulose residues are shown in Figure 3. After

421   bleaching step, all the three samples appear as regular fibre filaments and show a parallel

422   arrangement. Based on the obtained images, it seems that there is no great difference

423   between the three SC residues, except for the sample SC-225°C, which appears to have a

424   more irregular, jagged, and slightly damaged surface, probably as a result of the higher

425   temperature used in the reactor, which led to a partial cellulose degradation.

426

427   *3.3.4 X-ray analysis and crystallinity*

428   The XRD analysis on the straw cellulose obtained at the end of the entire lignocellulosic

429   fractionation process (SC-165°C, SC-195°C and SC-225°C), compared to the STD-

430   MCC, was carried out to establish if the obtained cellulose was crystalline or if its

431   morphological structure had been modified by the high AH temperatures.

432   All the cellulose samples obtained from WS show both crystalline and amorphous

433   regions. These regions are affected by the different pre-treatments applied to WS, as

434   shown in Figure 4.

435   Figure 4 shows a typical XRD measurement for cellulose samples from WS. All samples

436   show clear and strong diffraction peaks at around 14.2°, 23.3°, and 25.3°. In particular,

437   the intensity between peaks at 14.2° and 23.3° decreases when temperature increases,

438   with this showing how crystallinity increases with increasing temperatures.

439 Moreover, all the WS cellulose samples obtained at the end of the lignocellulosic

440 fractionation process showed similar spectra, which means that the different AH

441 temperatures do not cause changes in the structure of the obtained cellulose. However,

442 all three samples showed cellulose polymorph II structure, which is usually obtained

443 irreversibly from cellulose I through treatments with NaOH, and the extent of this

444 conversion is also influenced by the type of lignocellulosic feedstock used (Liu and Hu,

445 2008; Park et al., 2010); while the STD-MCC sample shows a polymorphic type I. Thus,

446 the parallel-chain crystal structure of the original cellulose I is converted into a more

447 stable anti-parallel arrangement of cellulose II (Moon et al., 2011); this indicates that

448 cellulose II should have better mechanical properties than cellulose I. Indeed, several

449 articles report that in film preparations, the type of polymorphism of cellulose influences

450 its reinforcing capacity and polymer-bonding capacity (Paukszta and Borysiak, 2013). In

451 particular, Dhar et al. (Dhar et al., 2015) reported that the incorporation of cellulose with

452 polymorphism II appreciably improved Young's modulus of PLA films, while their

453 elongation at break significantly decreased compared to cellulose I due to the formation

454 of an intertwined network of hydrogen bonds within the polymer matrix, resulting in

455 improved mechanical and barrier properties.

456 Based on this, all three cellulose samples obtained at the end of the lignocellulosic

457 fractionation process could be suitable for incorporation as reinforcing agents for

458 biodegradable packaging materials.

459 However, some authors (Borysiak and Grzątka-Zasadzińska, 2016; Paukszta and

460 Borysiak, 2013) reported better mechanical properties of the polymers containing

461 cellulose I. Therefore, it would be necessary to directly test both types of polymorphism

462 to assess any differences in the mechanical properties of the final material.

463 Furthermore, the degree of crystallinity of the final SC samples was also evaluated using

464 the peak fitting and deconvolution method. The degree of crystallinity (%) increases

465 slightly with increasing temperatures in the reactor, as a result of the degradation of

466 amorphous regions (66.33 ± 5.51^a, 70.33 ± 4.93^a and 85.67 ± 2.08^b for 165 °C, 195 °C

467 and 225 °C, respectively). However, all the produced samples were sufficiently

468 crystalline to reinforce different polymers. Nevertheless, by comparing the three

469 treatment conditions with the cellulose yields and the degree of crystallinity, the best

470 treatment condition turns out to be the one carried out at 195 °C. Indeed, since the SC-

471 225°C showed a very low cellulose yield (below 50%) we decided to take SC-195 °C

472 which presents a higher degree of crystallinity (about 70%) compared to SC-165°C.

473 Therefore, this cellulose (SC-195 °C) was tested in different percentages as a reinforcing

474 agent to produce PBAT-based films.

475

476 ## 3.4 *Film production*

477 ### *3.4.1 Mechanical and morphological properties of the PBAT/cellulose films*

478 The effect of adding SC-195°C on the mechanical properties of PBAT/cellulose films

479 was investigated, and the results are shown in Figure 5.

480 The values obtained for Young's modulus, tensile strength, and elongation at break of

481 PBAT films are in line with the values reported in the literature for this polymer and its

482 blends and composites (Deng et al., 2018; NUNES et al., 2017). The addition of 2 wt.%

483 STD-MCC did not influence the Young's modulus of the PBAT, whereas the addition of

484 SC-195°C at the same concentration led to a significant increase in the elastic modulus

485 of about 9 % compared to PBAT. At the same time, the modulus of the samples containing

486 5 wt.% cellulose further increased with both SC-195°C and STD-MCC without

487 significant differences. Similar results were observed for Young's modulus in

488 PBAT/TPS/MCC (Reis et al., 2014) and PLA/MCC composites (Haafiz et al., 2013). The

489 increase in modulus with increasing cellulose in PBAT can be attributed to the stiffening

490 action and high crystallinity index of the filler.

491   In addition, based on the obtained results, it seems that a filler addition of 5 wt.% leads

492   to an increase in Young's modulus, regardless of the type of polymorphism of the used

493   cellulose. In fact, the cellulose used as a control (STD-MCC, from Sigma-Aldrich)

494   presents a type I polymorphism, as reported by Paul et al. (Paul et al., 2021); whereas the

495   SC-195°C sample shows a type II polymorphism (Figure 4).

496   The Figure 5d clearly reveals that for all samples, the tensile strength decreases when the

497   amount of filler increases. The decrease is greater in films containing SC-195°C (reaching

498   a decrease of approximately 42% for both 2 and 5 wt.%, respectively, compared to pure

499   PBAT) than PBAT with STD-MCC (showing tensile strength decreases by 13% and 23%

500   for 2 and 5 wt.% addition, respectively). This result is probably due to the aggregation of

501   cellulose leading to a non-homogeneous dispersion of the filler in the polymer matrix,

502   especially with SC-195°C which presents a larger particle size than STD-MCC, or

503   because of poor interaction between the filler and the matrix (Haafiz et al., 2013). SEM

504   images included in Figure 6 agree with that observation. Figure 6 A-D shows that PBAT

505   composite films' surface presents a similar homogeneous aspect with some protuberances

506   for PBAT/SC-195°C and PBAT/STD-MCC at 2 and 5 wt.% of filler. However, Figure 6

507   E shows that at the cross-section, the films prepared with 5 wt.% of SC-195°C present a

508   bigger filler size when compared with STD-MCC (Figure 6 F).

509   Therefore, the difference observed in the tensile strength values between the SC-195°C

510   and STD-MCC samples does not seem to be related to the type of polymorphism of the

511   cellulose used, but rather to a different particle size of the employed powder.

512   The elongation at break of PBAT is also reduced with the incorporation of cellulose for

513   all samples. However, non-significant differences are observed between the two

514   concentrations tested; although, a greater reduction in elongation at break is observed

515   with SC-195°C (~28%) than with STD-MCC (~7%), compared to PBAT. These

516   observations of limitation in segmental chain movement of the PBAT during tensile

517   testing may be ascribed to the stiffening effect of the filler. The elongation at break may

518   be influenced by the quantity of the filler added, the interaction between the latter and the

519   matrix, and its dispersion in the matrix (Dhar et al., 2015; Haafiz et al., 2013).

520   The poor interaction and dispersion of cellulose in the matrix of PBAT due to the

521   tendency to agglomerate led to substantial local stress levels and decreased elongation at

522   break. A similar trend was observed in the study of Reis et al. (Reis et al., 2017), where

523   the TPS/PBAT-based film with higher concentrations of MCC (10%) exhibited lower

524   tensile strength (4.6 ± 0.1 MPa) and lower elongation at break (147 ± 34%). On the

525   contrary, Young's modulus values increased with increasing MCC concentration in the

526   film (reaching values of 79.2 ± 13.6 MPa with 10% MCC). Even in the research

527   conducted by Mathew et al. (Mathew et al., 2005) on PLA-based films, both tensile stress

528   and elongation at break were shown to be lower for composites than for pure PLA. The

529   authors showed that an increase in MCC content has a negative impact on the strength of

530   composites compared to pure PLA, whereas the modulus tends to increase with increasing

531   MCC content.

532   In summary, the SC obtained by AH at 195 °C behaves similarly to the STD-MCC when

533   used at 5 wt.%. In contrast, when added at 2 wt.%, SC-195°C produces a PBAT composite

534   with a higher elastic modulus than STD-MCC, even with the aggregation effects caused

535   by the different particle sizes. These results demonstrate that the process followed in this

536   work presents a great potential for the valorisation of WS waste to produce composites,

537   but also that it is still necessary to develop strategies to prevent particle aggregation and

538   favour a homogeneous dispersion of the filler in the matrix.

539

540   **4. Conclusions**

541   In the isolation of wheat straw cellulose with an autohydrolysis - alkaline hydrolysis -

542   bleaching process, autohydrolysis at 195 °C led to higher yield (83.5%), comparable

543 purity (~70%) and intermediate cellulose crystallinity (~70%) than at 165 °C and 225 °C.

544 Liquors from 195°C-AH showed higher monosaccharides and intermediate antioxidant

545 content. Straw cellulose obtained at the end of the entire fractionation process (SC-195°C)

546 starting from AH residue-195°C was tested at 2-5 wt.% as a reinforcement agent in

547 poly(butylene adipate-co-terephthalate) films, leading to increased Young's modulus and

548 decreased tensile strength and elongation at break. Future works should focus on the

549 valorisation of the AH liquors (e.g., in terms of hemicellulose, lignin or bioactive

550 compounds recovery), energy optimization of the process, of both autohydrolysis and

551 alkaline steps, and improvement of the tensile properties of the composite, enhancing

552 filler-polymer adhesion.

553

559

560 **References**

561 Abidi, N., Cabrales, L., Haigler, C.H., 2014. Changes in the cell wall and cellulose

562   content of developing cotton fibers investigated by FTIR spectroscopy. Carbohydr.

563   Polym. 100, 9–16. https://doi.org/10.1016/j.carbpol.2013.01.074

564 AOAC, 2007. Official Methods of Analysis, 18th ed.; The Association of Official

565   Analytical Chemist, Ed.; The Association of Official Analytical Chemist.

566 Arauzo, P.J., Lucian, M., Du, L., Olszewski, M.P., Fiori, L., Kruse, A., 2020. Improving

567   the recovery of phenolic compounds from spent coffee grounds by using

568   hydrothermal delignification coupled with ultrasound assisted extraction. Biomass

569   and Bioenergy 139. https://doi.org/10.1016/j.biombioe.2020.105616

570   Ballesteros, L.F., Ramirez, M.J., Orrego, C.E., Teixeira, J.A., Mussatto, S.I., 2017.

571   Optimization of autohydrolysis conditions to extract antioxidant phenolic

572   compounds from spent coffee grounds. J. Food Eng. 199, 1–8.

573   https://doi.org/10.1016/j.jfoodeng.2016.11.014

574   Bassani, A., Fiorentini, C., Vadivel, V., Moncalvo, A., Spigno, G., 2020.

575   Implementation of auto-hydrolysis process for the recovery of antioxidants and

576   cellulose from wheat straw. Appl. Sci. 10. https://doi.org/10.3390/app10176112

577   Bauer, J.L., Harbaum-Piayda, B., Schwarz, K., 2012. Phenolic compounds from

578   hydrolyzed and extracted fiber-rich by-products. LWT - Food Sci. Technol. 47,

579   246–254. https://doi.org/10.1016/j.lwt.2012.01.012

580   Borysiak, S., Grząbka-Zasadzińska, A., 2016. Influence of the polymorphism of

581   cellulose on the formation of nanocrystals and their application in

582   chitosan/nanocellulose composites. J. Appl. Polym. Sci. 133, 1–9.

583   https://doi.org/10.1002/app.42864

584   Botta, L., Titone, V., Mistretta, M.C., La Mantia, F.P., Modica, A., Bruno, M., Sottile,

585   F., Lopresti, F., 2021. PBAT based composites reinforced with microcrystalline

586   cellulose obtained from softwood almond shells. Polymers (Basel). 13.

587   https://doi.org/10.3390/polym13162643

588   Carvalheiro, F., Silva-Fernandes, T., Duarte, L.C., Gírio, F.M., 2009. Wheat straw

589   autohydrolysis: Process optimization and products characterization. Appl.

590   Biochem. Biotechnol. 153, 84–93. https://doi.org/10.1007/s12010-008-8448-0

591   Cheng, B., Wang, X., Lin, Q., Zhang, X., Meng, L., Sun, R.C., Xin, F., Ren, J., 2018.

592   New Understandings of the Relationship and Initial Formation Mechanism for

593   Pseudo-lignin, Humins, and Acid-Induced Hydrothermal Carbon. J. Agric. Food

594   Chem. 66, 11981–11989. https://doi.org/10.1021/acs.jafc.8b04754

595   De Abreu, D.A.P., Rodriguez, K.V., Cruz, J.M., 2012. Extraction, purification and

596   characterization of an antioxidant extract from barley husks and development of an

597   antioxidant active film for food package. Innov. Food Sci. Emerg. Technol. 13,

598   134–141. https://doi.org/10.1016/j.ifset.2011.10.003

599   Delbecq, F., Wang, Y., Muralidhara, A., El Ouardi, K.E., Marlair, G., Len, C., 2018.

600   Hydrolysis of hemicellulose and derivatives-a review of recent advances in the

601   production of furfural. Front. Chem. 6. https://doi.org/10.3389/fchem.2018.00146

602   Deng, Y., Yu, C., Wongwiwattana, P., Thomas, N.L., 2018. Optimising Ductility of

603   Poly(Lactic Acid)/Poly(Butylene Adipate-co-Terephthalate) Blends Through Co-

604   continuous Phase Morphology. J. Polym. Environ. 26, 3802–3816.

605   https://doi.org/10.1007/s10924-018-1256-x

606   Dhar, P., Tarafder, D., Kumar, A., Katiyar, V., 2015. Effect of cellulose nanocrystal

607   polymorphs on mechanical, barrier and thermal properties of poly(lactic acid)

608   based bionanocomposites. RSC Adv. 5, 60426–60440.

609   https://doi.org/10.1039/c5ra06840a

610   Fernández-Cegrí, V., Ángeles de la Rubia, M., Raposo, F., Borja, R., 2012. Effect of

611   hydrothermal pretreatment of sunflower oil cake on biomethane potential focusing

612   on fibre composition. Bioresour. Technol. 123, 424–429.

613   https://doi.org/10.1016/j.biortech.2012.07.111

614   Garrote, G., Cruz, J.M., Domínguez, H., Parajó, J.C., 2003. Valorisation of waste

615   fractions from autohydrolysis of selected lignocellulosic materials. J. Chem.

616   Technol. Biotechnol. 78, 392–398. https://doi.org/10.1002/jctb.760

617   Garrote, G., Cruz, J.M., Moure, A., Domínguez, H., Parajó, J.C., 2004. Antioxidant

618   activity of byproducts from the hydrolytic processing of selected lignocellulosic

619   materials. Trends Food Sci. Technol. 15, 191–200.

620   https://doi.org/10.1016/j.tifs.2003.09.016

621 Garrote, G., Domínguez, H., Parajó, J.C., 2001. Generation of xylose solutions from

622   Eucalyptus globulus wood by autohydrolysis-posthydrolysis processes:

623   Posthydrolysis kinetics. Bioresour. Technol. 79, 155–164.

624   https://doi.org/10.1016/S0960-8524(01)00044-X

625 Haafiz, M.K.M., Hassan, A., Zakaria, Z., Inuwa, I.M., Islam, M.S., Jawaid, M., 2013.

626   Properties of polylactic acid composites reinforced with oil palm biomass

627   microcrystalline cellulose. Carbohydr. Polym. 98, 139–145.

628   https://doi.org/10.1016/j.carbpol.2013.05.069

629 Hu, F., Jung, S., Ragauskas, A., 2012. Pseudo-lignin formation and its impact on

630   enzymatic hydrolysis. Bioresour. Technol. 117, 7–12.

631   https://doi.org/10.1016/j.biortech.2012.04.037

632 Hubbe, M.A., Pizzi, A., Zhang, H., Halis, R., 2018. Critical links governing

633   performance of self-binding and natural binders for hot-pressed reconstituted

634   lignocellulosic board without added formaldehyde: A review. BioResources 13,

635   2049–2115. https://doi.org/10.15376/biores.13.1.Hubbe

636 Jin, E., Guo, J., Yang, F., Zhu, Y., Song, J., Jin, Y., Rojas, O.J., 2016. On the

637   polymorphic and morphological changes of cellulose nanocrystals (CNC-I) upon

638   mercerization and conversion to CNC-II. Carbohydr. Polym. 143, 327–335.

639   https://doi.org/10.1016/j.carbpol.2016.01.048

640 Kalia, S., Dufresne, A., Cherian, B.M., Kaith, B.S., Avérous, L., Njuguna, J.,

641   Nassiopoulos, E., 2011. Cellulose-based bio- and nanocomposites: A review. Int. J.

642   Polym. Sci. 2011. https://doi.org/10.1155/2011/837875

643 Kaparaju, P., Felby, C., 2010. Characterization of lignin during oxidative and

644   hydrothermal pre-treatment processes of wheat straw and corn stover. Bioresour.

645   Technol. 101, 3175–3181. https://doi.org/10.1016/j.biortech.2009.12.008

646   Kootstra, A.M.J., Beeftink, H.H., Scott, E.L., Sanders, J.P.M., 2009. Comparison of

647   dilute mineral and organic acid pretreatment for enzymatic hydrolysis of wheat

648   straw. Biochem. Eng. J. 46, 126–131. https://doi.org/10.1016/j.bej.2009.04.020

649   Lee, H.V., Hamid, S.B.A., Zain, S.K., 2014. Conversion of lignocellulosic biomass to

650   nanocellulose: Structure and chemical process. Sci. World J. 2014.

651   https://doi.org/10.1155/2014/631013

652   Liu, R., Yu, H., Huang, Y., 2005. Structure and morphology of cellulose in wheat straw.

653   Cellulose 12, 25–34. https://doi.org/10.1007/s10570-004-0955-8

654   Liu, Y., Hu, H., 2008. X-ray diffraction study of bamboo fibers treated with NaOH.

655   Fibers Polym. 9, 735–739. https://doi.org/10.1007/s12221-008-0115-0

656   Mathew, A.P., Oksman, K., Sain, M., 2005. Mechanical properties of biodegradable

657   composites from poly lactic acid (PLA) and microcrystalline cellulose (MCC). J.

658   Appl. Polym. Sci. 97, 2014–2025. https://doi.org/10.1002/app.21779

659   Miron, J., Ben-Ghedalia, D., 1982. Effect of hydrolysing and oxidizing agents on the

660   composition and degradation of wheat straw monosaccharides. Eur. J. Appl.

661   Microbiol. Biotechnol. 15, 83–87. https://doi.org/10.1007/BF00499511

662   Moon, R.J., Martini, A., Nairn, J., Simonsen, J., Youngblood, J., 2011. Cellulose

663   nanomaterials review: Structure, properties and nanocomposites, Chemical Society

664   Reviews. https://doi.org/10.1039/c0cs00108b

665   NUNES, E. de C.D., SOUZA, A.G. de, COIADO, R.D.S., MOURA, E.A.B., ROSA, D.

666   dos S., 2017. Evaluation of the poly (lactic acid) and calcium carbonate effects on

667   the mechanical and morphological properties in PBAT blends and composites. Int.

668   J. Innov. Sci. Eng. Technol.

669   Oefner, P.J., Lanziner, A.H., Bonn, G., Bobleter, O., 1992. Quantitative studies on

670   furfural and organic acid formation during hydrothermal, acidic and alkaline

671   degradation of D-xylose. Monatshefte für Chemie Chem. Mon. 123, 547–556.

672   https://doi.org/10.1007/BF00816848

673   Park, S., Baker, J.O., Himmel, M.E., Parilla, P.A., Johnson, D.K., 2010. Cellulose

674   crystallinity index: Measurement techniques and their impact on interpreting

675   cellulase performance. Biotechnol. Biofuels 3. https://doi.org/10.1186/1754-6834-

676   3-10

677   Paukszta, D., Borysiak, S., 2013. The influence of processing and the polymorphism of

678   lignocellulosic fillers on the structure and properties of composite materials-A

679   review. Materials (Basel). 6, 2747–2767. https://doi.org/10.3390/ma6072747

680   Paul, U.C., Fragouli, D., Bayer, I.S., Zych, A., Athanassiou, A., 2021. Effect of Green

681   Plasticizer on the Performance of Microcrystalline Cellulose/Polylactic Acid

682   Biocomposites. ACS Appl. Polym. Mater. https://doi.org/10.1021/acsapm.1c00281

683   Pérez, J.A., González, A., Oliva, J.M., Ballesteros, I., Manzanares, P., 2007. Effect of

684   process variables on liquid hot water pretreatment of wheat straw for

685   bioconversion to fuel-ethanol in a batch reactor. J. Chem. Technol. Biotechnol. 82,

686   929–938. https://doi.org/10.1002/jctb.1765

687   Ramos, E., Calatrava, S.F., Jiménez, L., 2008. Bleaching with hydrogen peroxide. A

688   review. Afinidad 65, 366–373.

689   Rasheed, M., Jawaid, M., Parveez, B., Bhat, A.H., Alamery, S., 2021. Morphology,

690   structural, thermal, and tensile properties of bamboo microcrystalline

691   cellulose/poly(Lactic acid)/poly(butylene succinate) composites. Polymers (Basel).

692   13, 1–15. https://doi.org/10.3390/polym13030465

693   Reis, M.O., Olivato, J.B., Zanela, J., Yamashita, F., Grossmann, M.V.E., 2017.

694   Influence of microcrystalline cellulose in thermoplastic starch/polyester blown

695   films. Polimeros 27, 129–135. https://doi.org/10.1590/0104-1428.2338

696   Reis, M.O., Zanela, J., Olivato, J., Garcia, P.S., Yamashita, F., Grossmann, M.V.E.,

697   2014. Microcrystalline Cellulose as Reinforcement in Thermoplastic

698   Starch/Poly(butylene adipate-co-terephthalate) Films. J. Polym. Environ. 22, 545–

699   552. https://doi.org/10.1007/s10924-014-0674-7

700   Ruiz, H.A., Ruzene, D.S., Silva, D.P., Quintas, M.A.C., Vicente, A.A., Teixeira, J.A.,

701   2011. Evaluation of a hydrothermal process for pretreatment of wheat straw-effect

702   of particle size and process conditions. J. Chem. Technol. Biotechnol. 86, 88–94.

703   https://doi.org/10.1002/jctb.2518

704   Saleem Khan, T., Mubeen, U., 2012. Wheat Straw: A Pragmatic Overview. Curr. Res. J.

705   Biol. Sci. 4, 673–675.

706   Shinde, S.D., Meng, X., Kumar, R., Ragauskas, A.J., 2018. Recent advances in

707   understanding the pseudo-lignin formation in a lignocellulosic biorefinery. Green

708   Chem. 20, 2192–2205. https://doi.org/10.1039/c8gc00353j

709   Sidiras, D., Batzias, F., Ranjan, R., Tsapatsis, M., 2011. Simulation and optimization of

710   batch autohydrolysis of wheat straw to monosaccharides and oligosaccharides.

711   Bioresour. Technol. 102, 10486–10492.

712   Sluiter, A., Hames, B., Ruiz, R., Scarlata, C., Sluiter, J., Templeton, D., 2010.

713   Determination of structural carbohydrates and lignin in biomass determination of

714   structural carbohydrates and lignin in biomass. Natl. Renew. Energy Lab.

715   https://doi.org/NREL/TP-510-42618

716   Sun, X.-F., Sun, R., Fowler, P., Baird, M.S., 2005. Extraction and characterization of

717   original lignin and hemicelluloses from wheat straw. J. Agric. Food Chem. 53,

718   860–870. https://doi.org/10.1021/jf040456q

719   Sun, Y., Cheng, J., 2002. Hydrolysis of lignocellulosic materials for ethanol production:

720   A review. Bioresour. Technol. 83, 1–11. https://doi.org/10.1016/S0960-

721   8524(01)00212-7

722   Tilay, A., Bule, M., Kishenkumar, J., Annapure, U., 2008. Preparation of ferulic acid

723   from agricultural wastes: Its improved extraction and purification. J. Agric. Food

724   Chem. 56, 7644–7648. https://doi.org/10.1021/jf801536t

725 Trache, D., Hussin, M.H., Hui Chuin, C.T., Sabar, S., Fazita, M.R.N., Taiwo, O.F.A.,

726   Hassan, T.M., Haafiz, M.K.M., 2016. Microcrystalline cellulose: Isolation,

727   characterization and bio-composites application—A review. Int. J. Biol.

728   Macromol. 93, 789–804. https://doi.org/10.1016/j.ijbiomac.2016.09.056

729 Vadivel, V., Moncalvo, A., Dordoni, R., Spigno, G., 2017. Effects of an acid/alkaline

730   treatment on the release of antioxidants and cellulose from different agro-food

731   wastes. Waste Manag. 64, 305–314. https://doi.org/10.1016/j.wasman.2017.03.010

732 Wüst, D., Correa, C.R., Jung, D., Zimmermann, M., Kruse, A., Fiori, L., 2020.

733   Understanding the influence of biomass particle size and reaction medium on the

734   formation pathways of hydrochar. Biomass Convers. Biorefinery 10, 1357–1380.

735   https://doi.org/10.1007/s13399-019-00488-0

736 Zhang, J., Deng, H., Sun, Y., Pan, C., Liu, S., 2010. Isolation and characterization of

737   wheat straw lignin with a formic acid process. Bioresour. Technol. 101, 2311–

738   2316. https://doi.org/10.1016/j.biortech.2009.11.037

739

740 Table 1 Chemical composition of wheat straw used in this study. Results, except moisture, are expressed
741 as weight percentage on a dry weight basis and reported as mean ± standard deviation. *Obtained with the
742 conversion factor of 5.83.

Component	Wheat straw
Moisture (g/100 g)	8.65 ± 0.04
Ash (g/100 g_{dm})	5.7 ± 0.3
Protein* (g/100 g_{dm})	4.5 ± 0.4
Lipid (g/100 g_{dm})	1.3 ± 0.1
Total Lignin (g/100 g_{dm})	21.3 ± 1.0
Cellulose (g/100 g_{dm})	31.5 ± 0.9
Hemicellulose (g/100 g_{dm})	15.4 ± 1.4

743

744 Table 2 Recovery mass yields (%) of each step of the process of Figure 1 and recovery mass yields of the
745 entire process (% total). Values reported as mean ± standard deviation. Values reported different lowercase
746 letters are significantly different ($p < 0.05$).

Treatment temperature °C	MASS YIELDS			
	% Autohydrolysis	% Alkaline hydrolysis	% Bleaching	% Total
165 °C	77.5 ± 3.3[a]	52.4 ± 9.8[a]	90.4 ± 4.6[a]	36.4 ± 5.0[a]
195 °C	60.9 ± 2.7[b]	74.6 ± 2.9[b]	84.8 ± 1.1[a]	38.5 ± 0.6[a]
225 °C	53.3 ± 0.5[c]	58.8 ± 3.7[a]	68.1 ± 1.7[b]	21.4 ± 1.6[b]

747

748 Table 3 Total phenolic content (TPC) and antioxidant activity (evaluated with FRAP and ABTS assays) of
749 autohydrolysis liquors obtained at 3 different temperatures (165, 195 and 225 °C). Values expressed on WS
750 dry matter as mean ± standard deviation. GAE: gallic acid equivalent. Tr: Trolox. Values reported different
751 lowercase letters are significantly different (p < 0.05).

Treatment temperature °C	TPC mgGAE/gWS$_{dm}$	FRAP μmolFe(II)/gWS$_{dm}$	ABTS μmolTr/gWS$_{dm}$
165 °C	11.4 ± 0.9^a	49.2 ± 2.7^a	62.0 ± 5.0^a
195 °C	24.3 ± 2.0^b	167.4 ± 14.0^b	105.6 ± 12.4^b
225 °C	30.6 ± 1.7^c	206.5 ± 12.9^c	136.8 ± 7.4^c

752

753 Table 4 Monosaccharide's release of autohydrolysis liquors obtained at three different temperatures (165,
754 195 and 225 °C). Values reported as mean ± standard deviation. Values reported different lowercase letters
755 are significantly different (p < 0.05).

Treatment temperature °C	pH	Acetic acid g/L	Free glucose (mg/L)	Free xylose (mg/L)	Free arabinose (mg/L)
165 °C	4.9 ± 0.1^a	0.6 ± 0.1^a	88.5 ± 10.0^a	85.2 ± 8.2^a	241.6 ± 3.5^a
195 °C	4.2 ± 0.1^b	1.1 ± 0.1^b	95.0 ± 9.4^a	253.6 ± 31.2^b	192.0 ± 20.3^b
225 °C	3.74 ± 0.03^a	1.41 ± 0.04^c	87.7 ± 2.8^a	21.9 ± 1.5^c	Not detected^c

756

757 Table 5 Comparison of structural carbohydrates of solid obtained after the autohydrolysis and bleaching
758 steps. The recovery yields (%) were expressed by calculating the ratio between the content of cellulose,
759 hemicellulose, and lignin, respectively, after the process steps and the initial content in WS dry matter.
760 Values reported as mean ± standard deviation. Values reported different lowercase letters are significantly
761 different ($p < 0.05$). *Calculated by difference.

STRUCTURAL CARBOHYDRATES	AFTER AUTOHYDROLYSIS			AFTER BLEACHING		
	165 °C	195 °C	225 °C	165 °C	195 °C	225 °C
% Cellulose recovery	89.0±4.5[a]	90.3±2.6[a]	77.5±5.5[b]	79.5±10.8[a]	83.5±5.5[a]	48.5±4.3[b]
% Hemicellulose recovery	45.4±0.5[a]	6.9±1.5[b]	1.5±0.3[c]	4.8±0.9[a]	1.9±0.3[b]	0.17±0.01[c]
% Total lignin recovery	58.9±12.8[a]	74.3±3.0[ab]	90.9±2.7[b]	16.7±2.7[ab]	22.2±2.8[a]	10.8±1.6[b]
% Cellulose content of solid residue	38.0±0.7[a]	46.7±3.0[b]	45.7±3.6[b]	68.1±1.6[a]	69.83±0.04[a]	73.0±1.1[b]
% Hemicellulose content of solid residue	9.1±0.5[a]	1.7±0.3[b]	0.37±0.01[c]	2.0±0.1[a]	0.7±0.1[b]	0.12±0.01[c]
% Acid soluble lignin	1.0±0.1[a]	1.6±0.1[b]	2.0±0.2[c]	0.54±0.02[a]	0.44±0.04[b]	0.43±0.02[b]
% Acid insoluble lignin	15.3±4.0[a]	24.5±2.0[b]	34.3±1.0[c]	9.1±0.6[a]	11.8±1.4[a]	10.3±1.9[a]
% Total Lignin content of solid residue	16.3±4.0[a]	26.1±2.1[b]	36.3±0.9[c]	9.7±0.6[a]	12.2±1.4[a]	10.8±1.8[a]
% Other content of solid residue*	36.6	27.1	17.63	20.2	17.27	16.08

762

763

```
         ┌─────────────────┐
         │  WHEAT STRAW    │  Milled with a hammer mill + 2 mm sieve
         └─────────────────┘
                  │
         ┌─────────────────┐   ➤ 1:20 WS:H₂O (w/v)
         │ AUTOHYDROLYSIS  │   ➤ 3 different T tested: 165 °C, 195 °C and 225 °C, 15 min, 180 rpm
         └─────────────────┘
                  │
         ┌─────────────────┐
         │   FILTRATION    │   Whatman filter paper (N° 589/2)
         └─────────────────┘
            │          │                    ┌ · · · · · · · · · · · · · · · · · ┐
   ┌──────────┐   ┌──────────┐                • Recovery mass yields
   │ LIQUOR   │   │  SOLID   │                • Structural carbohydrates
   └──────────┘   └──────────┘                • FTIR spectroscopic
 ┌ · · · · · · · ┐     │                      • X-ray analysis
   • TPC              │              └ · · · · · · · · · · · · · · · · · ┘
   • Antioxidant  ┌─────────────────┐
     activity     │ DRYING 60 °C x 24 h │
   • Sugar        └─────────────────┘
     composition        │
   • Acetic acid  ┌─────────────────┐   ➤ 1:20 solid:4N NaOH (w/v), room T, 150 rpm, 24 h
     content      │    ALKALINE     │
 └ · · · · · · · ┘│   HYDROLYSIS    │
                  └─────────────────┘
                         │
                  ┌─────────────────┐
                  │   FILTRATION    │   Whatman filter paper (N° 589/2)
                  └─────────────────┘
                    │          │
           ┌──────────────┐  ┌──────────┐  ┌ · · · · · · · · · · · · · · ┐
           │ BASIC LIQUOR │  │  SOLID   │    • Recovery mass yields
           └──────────────┘  └──────────┘  └ · · · · · · · · · · · · · · ┘
                                  │
                  ┌─────────────────────┐
                  │  WASHING WITH H₂O   │
                  │    UNTIL pH = 7     │
                  └─────────────────────┘
                         │
                  ┌─────────────────┐
                  │ DRYING 60 °C x 24 h │
                  └─────────────────┘
                         │
                  ┌─────────────────┐   ➤ 1:20 solid:5% H₂O₂ (v/v), 45 °C, 120 rpm, 8 h, pH 11.5
                  │    BLEACHING    │   ➤ Static cooling, room T, 24 h
                  └─────────────────┘
                         │
                  ┌─────────────────┐
                  │   FILTRATION    │   Whatman filter paper (N° 589/2)
                  └─────────────────┘
                    │          │
        ┌──────────────────┐  ┌──────────┐
        │ BLEACHING LIQUOR │  │  SOLID   │
        └──────────────────┘  └──────────┘
                                  │
                  ┌─────────────────────┐
                  │   WASHING WITH      │
                  │  50% ACETIC ACID    │
                  └─────────────────────┘
                         │
                  ┌─────────────────────┐
                  │  WASHING WITH H₂O   │
                  │    UNTIL pH = 7     │
                  └─────────────────────┘
                         │
                  ┌─────────────────┐
                  │ DRYING 60 °C x 24 h │
                  └─────────────────┘
                         │                 ┌ · · · · · · · · · · · · · · · · · ┐
                  ┌─────────────────┐        • Recovery mass yields
                  │   CELLULOSE     │        • Structural carbohydrates
                  └─────────────────┘        • FTIR spectroscopic
                                             • X-ray analysis
                                             • SEM observation
                                           └ · · · · · · · · · · · · · · · · · ┘
```

764
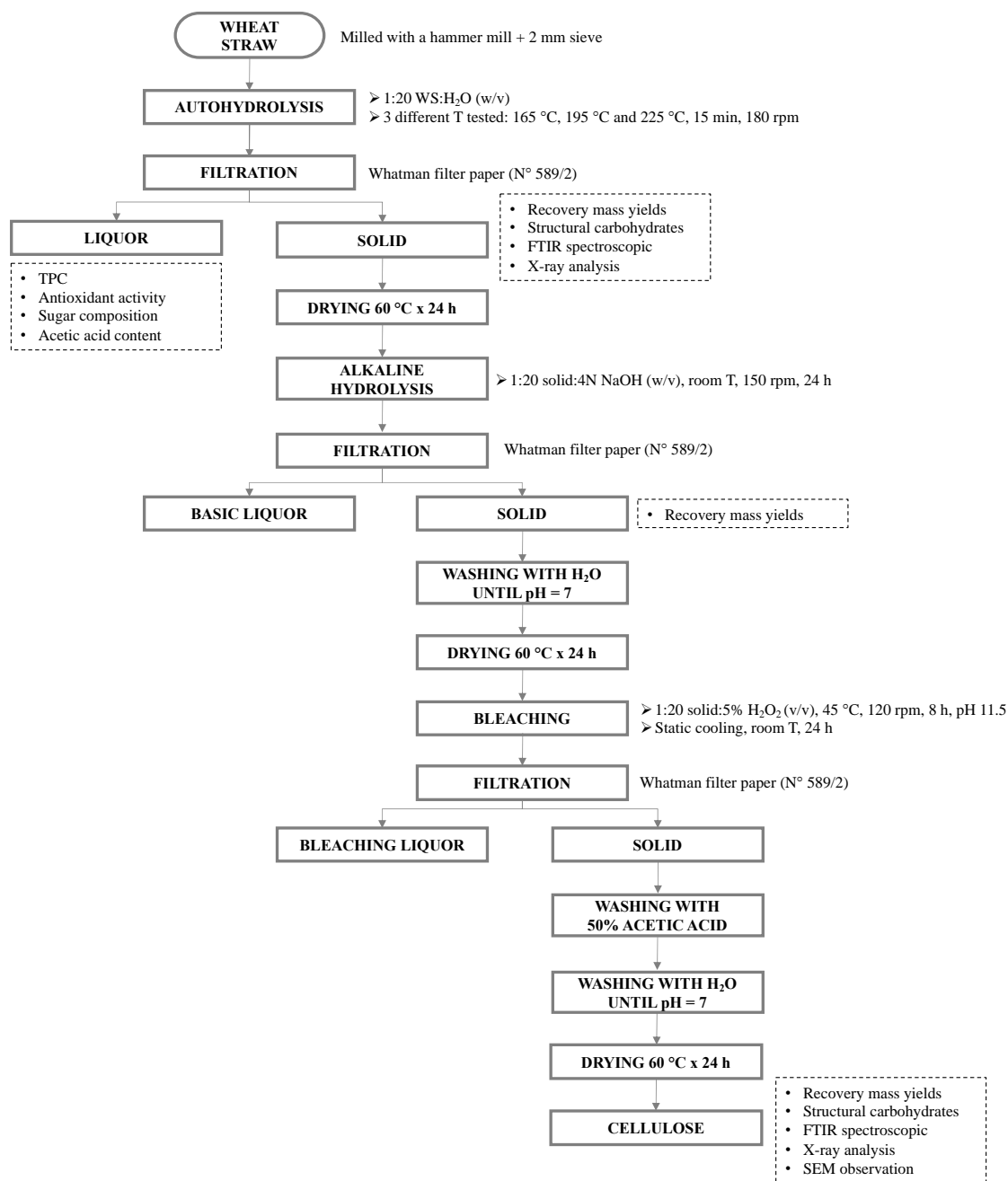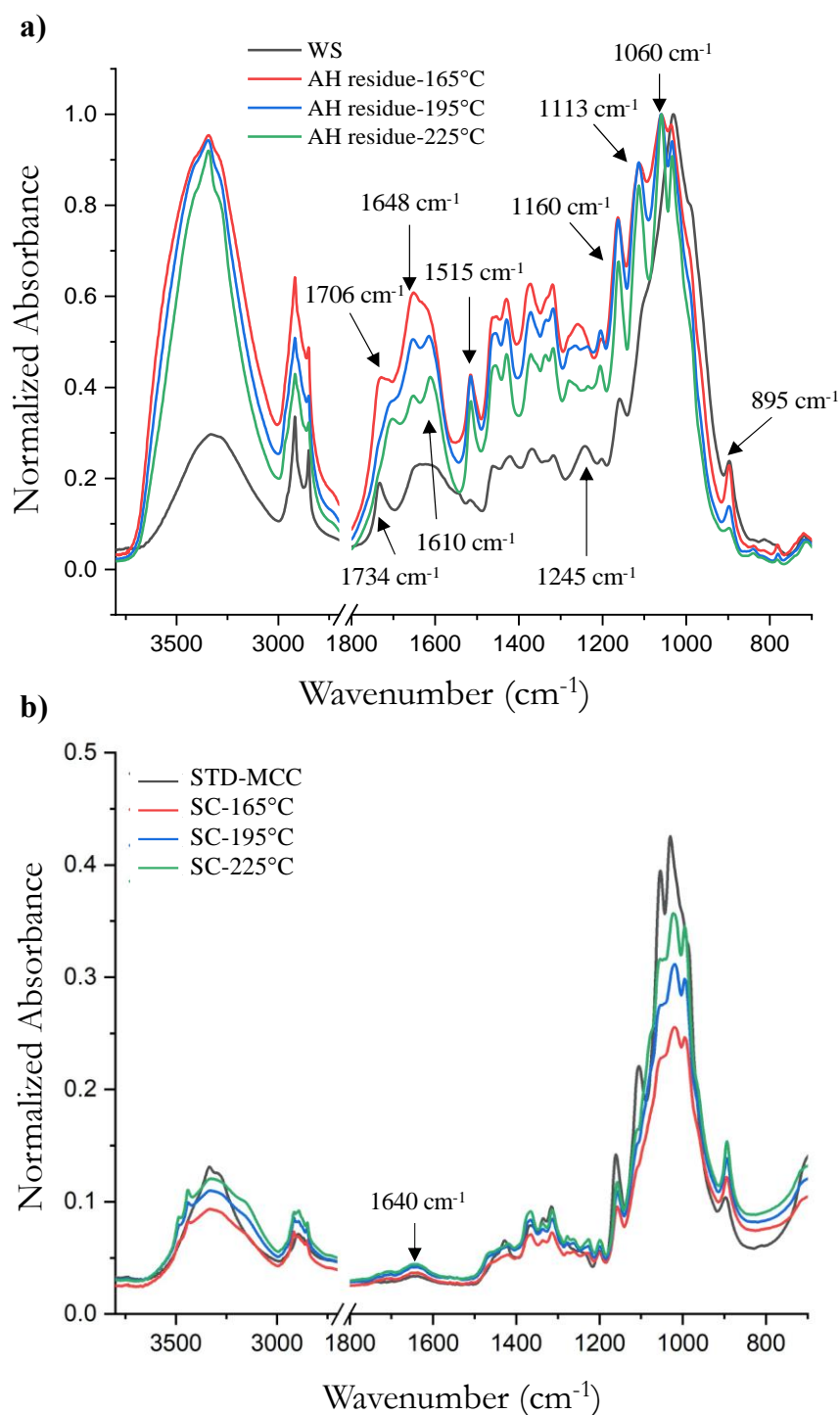765   Figure 1 Scheme of the lignocellulosic fraction process applied in this study to recover cellulose from WS.

766

a) The FTIR spectra of WS and the three samples obtained after the autohydrolysis step (AH residues-165, 195 and 225°C). b) FTIR spectra of the three straw cellulose obtained at the end of the entire lignocellulosic fractionation process (SC-165, SC-195 and SC-225°C) in comparison with commercial microcrystalline cellulose STD-MCC (black line).
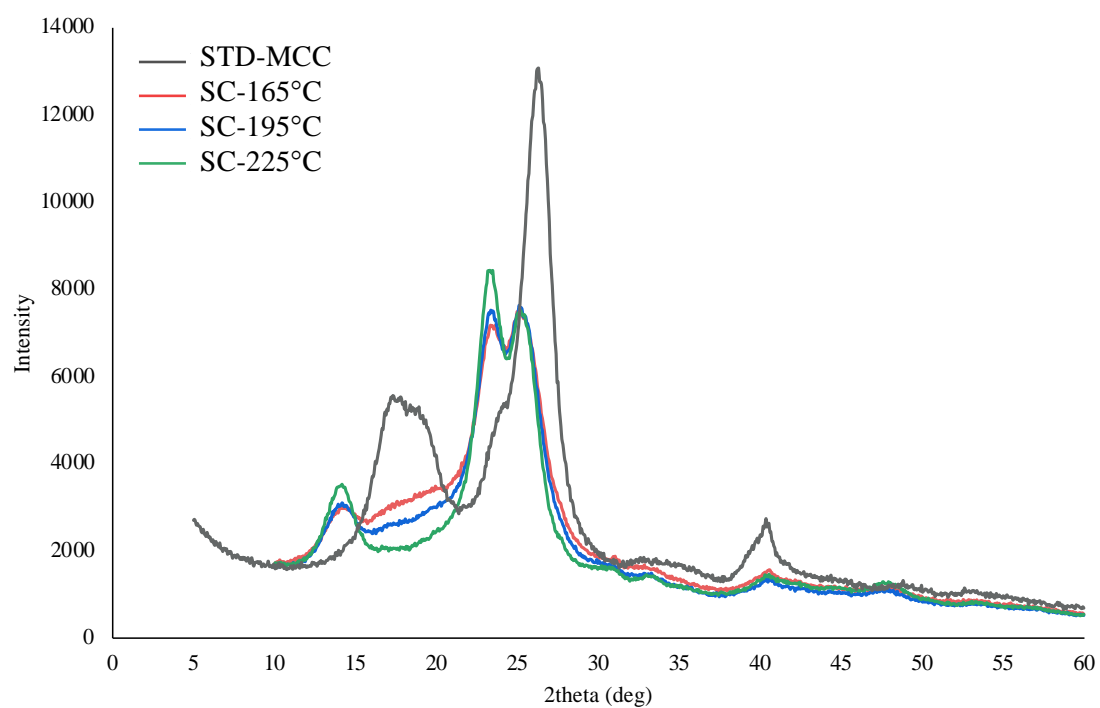
773
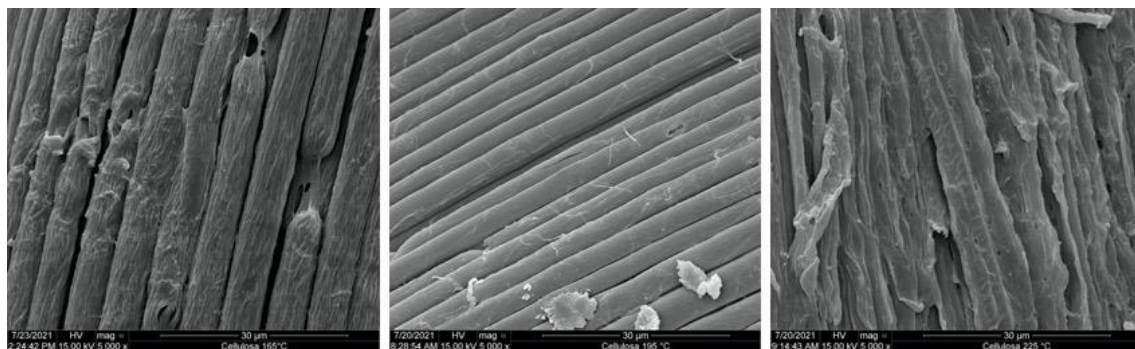
774
775 Figure 3 SEM observation of SC-165°C, SC-195°C and SC-225°C, respectively.

776

777

778
779 Figure 4 Typical X-ray diffraction measurement results (CoKα) for WS cellulose residues obtained through
780 the different autohydrolysis treatments (at 165, 195 and 225 °C) compared to a STD-MCC sample.
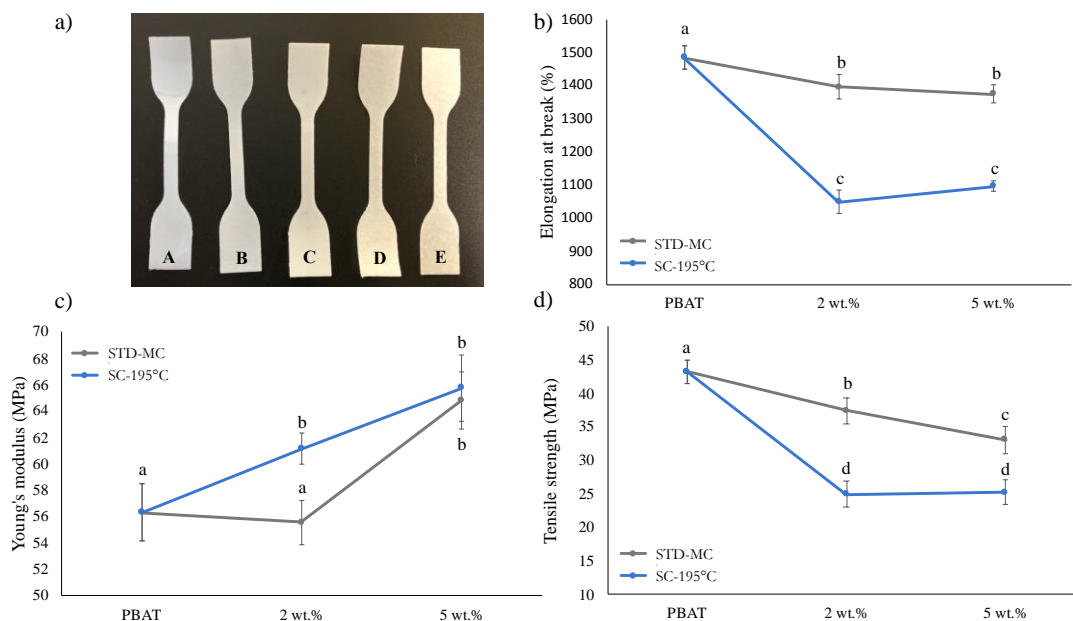
781

782

783
784 Figure 5 Mechanical properties of pure PBAT films and of PBAT films with different concentrations of
785 cellulose (2 and 5 wt.%). Blue line: straw cellulose (SC) obtained at the end of the entire fractionation
786 process (SC-195°C) starting from AH residue-195°C; grey line: commercial microcrystalline cellulose
787 (STD-MCC). a) Dumbbell samples used for mechanical testing: (A) PBAT, (B) PBAT/STD-MCC-2, (C)
788 PBAT/STD-MCC-5, (D) PBAT/SC-195°C-2, (E) PBAT/SC-195°C-5; b) Elongation at break (%); c)
789 Young's modulus (MPa); d) Tensile strength (MPa). Values reported different lowercase letters are
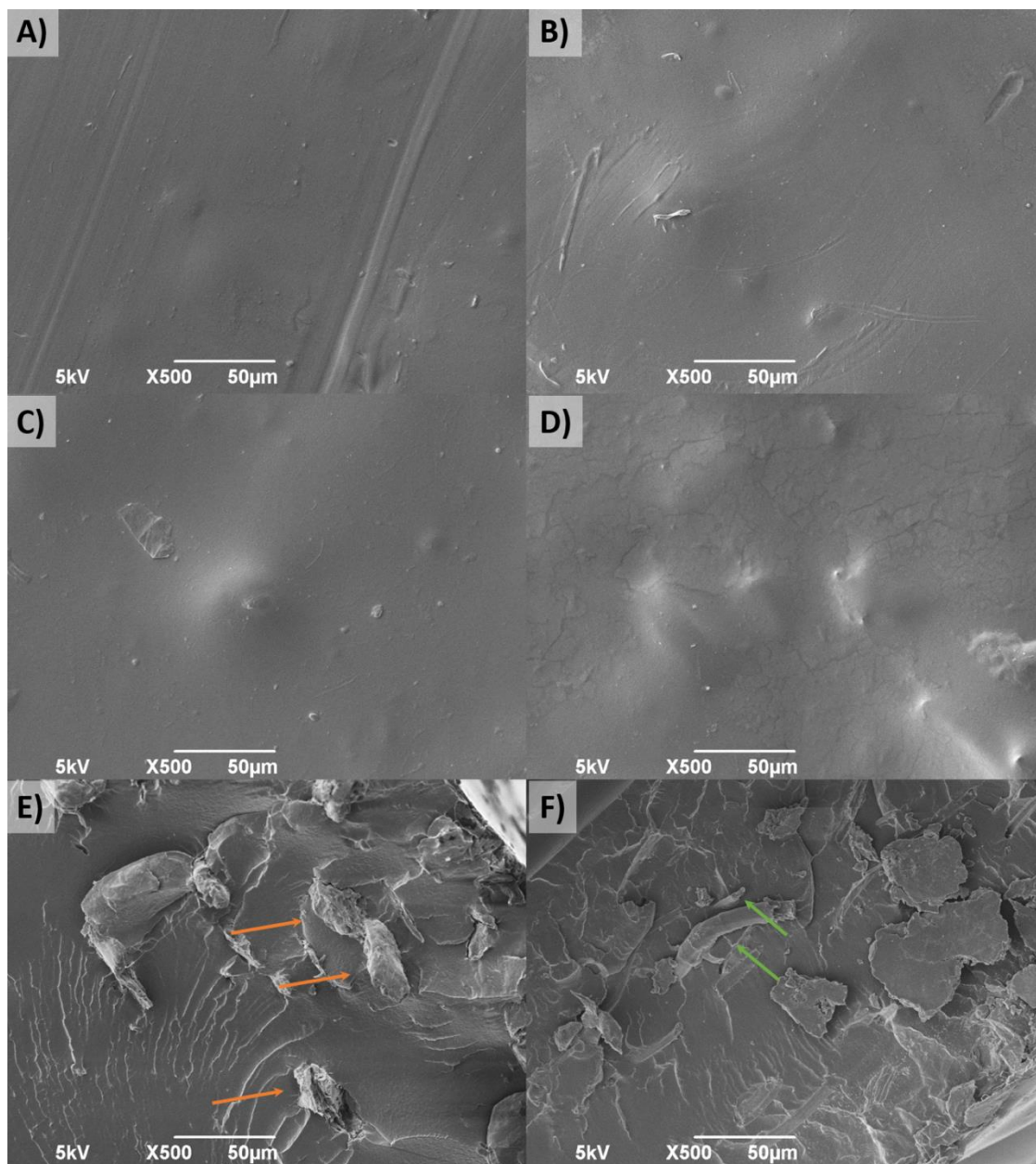790 significantly different (p < 0.05).

Figure 6 SEM image of the PBAT films with different concentrations of cellulose, from straw cellulose (SC) obtained at the end of the entire fractionation process (SC-195°C) starting from AH residue-195°C, or commercial microcrystalline cellulose (STD-MCC). A) PBAT with 2% STD-MCC; B) PBAT with 2% SC-195°C; C) PBAT with 5% STD-MCC; D) PBAT with 5% SC-195°C; E) cross section of PBAT with 5% STD-MCC, cellulose filler is highlighted with orange arrows; F) cross section of PBAT with 5% SC-195°C, cellulose filler is highlighted with green arrows.